Supporting Information

Scott A. Gabel[‡], Michael R. Duff[§], Lars C. Pedersen[‡], Eugene F. DeRose[‡], Juno M. Krahn, Elizabeth E. Howell[§], Robert E. London*[‡]

[‡]Genome Integrity and Structural Biology Laboratory

National Institute of Environmental Health Sciences, NIH

111 T. W. Alexander Dr.

Research Triangle Park, NC 27709

[§]Department of Biochemistry, Cellular & Molecular Biology

University of Tennessee

Knoxville, TN 37996

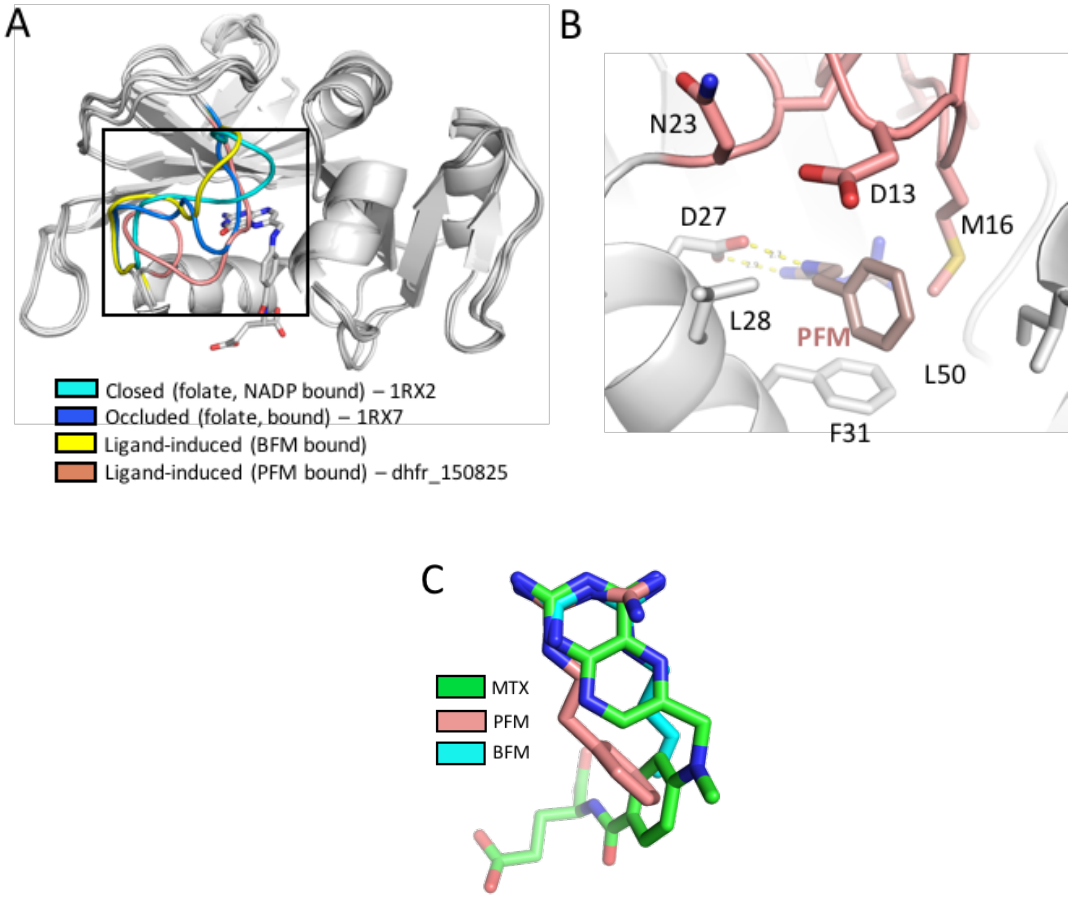

Figure S1. Ligand-induced conformations of the Met20 loop and biguanide positions. A) Overlaid ribbon diagrams of ecDHFR complexes, with the bound folate shown in gray. The colored loops correspond to residues I14-N23 with color coding: folate-$NADP^+$ (cyan, pdb: 1RX2), folate (blue, pdb: 1RX7), BFM (yellow), and PFM (beige). The ligand-induced conformations of the Met20 loop each differ. B) Expanded view of the PFM complex exhibiting a completely unique conformation in which Met16 enters the active site and interacts directly with the phenethyl group of the PFM. C) Despite the different alkyl substitution patterns, both the phenethyl and N-butyl groups partially fill the space occupied by the p-aminobenzoyl group of MTX. Steric conflict in PFM and, to a lesser extent, BFM, is relieved by rotation of the planes containing the two guanidino groups of the biguanides. The MTX complex corresponds to pdb: 1RA3 [1].

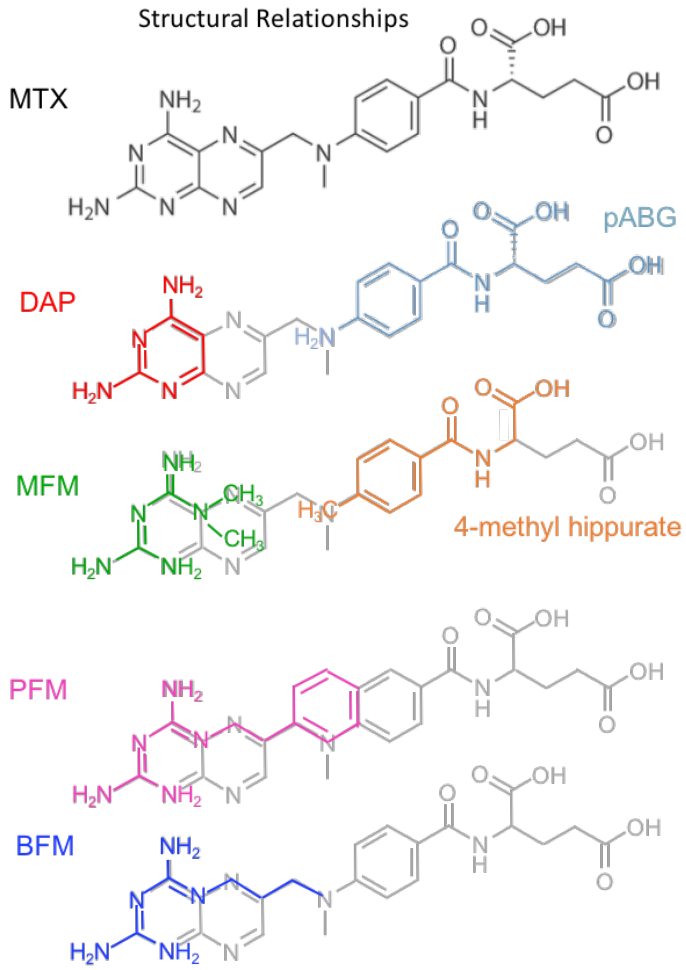

Figure S2. Structural relationships of DHFR ligands to methotrexate. As pointed out by Birdsall et al. [2], 2,4-diaminpyrimidine (DAP) and pABG can be viewed as components of MTX. Metformin (MFM) and hippurate analogs such as 4-methylhippurate approximate these components, and were hypothesized to interact with the same subsites to which DAP and pABG bind. BFM and PFM bind primarily to the pteridine-binding subsite, but include substituents that extend into the pABG-binding subsite.

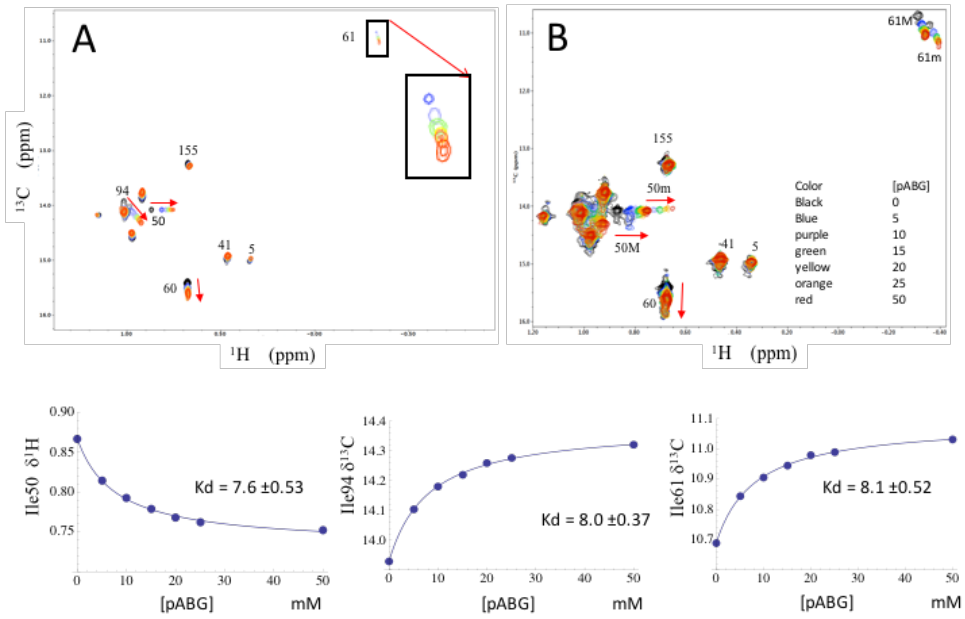

Figure S3. Titration of pABG into a sample of [$^{13}CH_3$-Ile]ecDHFR. A) ^{1}H-^{13}C HSQC spectra of [$^{13}CH_3$-Ile]ecDHFR as a function of added pABG. The most significantly shifted resonances correspond to Ile50, Ile61, and Ile94. The color coded concentrations in mM are: 0 (black), 5 (blue) 10 (purple), 15 (green), 20 (yellow), 25 (orange), 50 (red). B) Lower threshold plot capturing the minor resonances. Minor resonances for Ile61 and Ile50 are resolved. Note that for Ile50, the endpoint of the pABG titration overlays the first point of the minor resonance. The pABG binding affinity was apparently identical for the major and minor species. Minor conformation(s) of DHFR have been noted in previous studies [3]. C) *Mathematica* fits of the most sensitive Ile resonances yield a mean K_d of 7.9 mM.

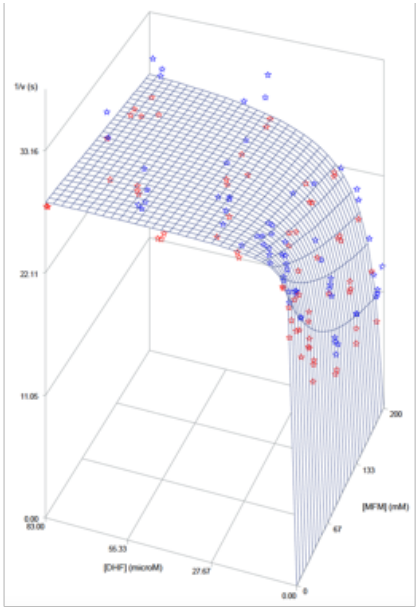

Parameter Estimates								
Parameter	Estimate	Standard Error	DF	t Value	Pr > |t|	95% Confidence Limits		Gradient
KmA	0.3946	0.06869	135	5.74	<.0001	0.2587	0.5304	-0.01413
kcat	28.6279	0.2824	135	101.37	<.0001	28.0694	29.1864	-0.00271
Ki	17.8848	3.5194	135	5.08	<.0001	10.9246	24.8450	0.000311
s2e	3.2721	0.3982	135	8.22	<.0001	2.4845	4.0597	-0.00162

Figure S4. Global fit of the metformin inhibition data with SAS software. The plot above corresponds to a global fit using model CI: Predicted reaction rates when enzyme=1. R^2 = 90.1%; K_i = 17.9 ±3.2 mM. Fitting procedure as described previously [4].

A) 0.1 mM ecDHFR, 5 mM 4-methylhippurate, 5 mM MFM

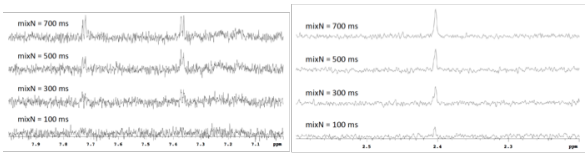

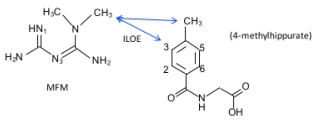

B) 0.1 mM ecDHFR, 5 mM MFM, 5 mM 4-Bromohippurate

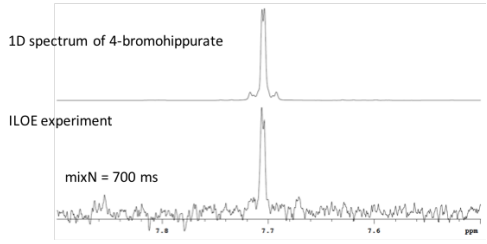

C) 0.1 mM ecDHFR, 5 mM 3-4-oxo-4-(2,3,4,5-tetramethylbenzoyl)propionate

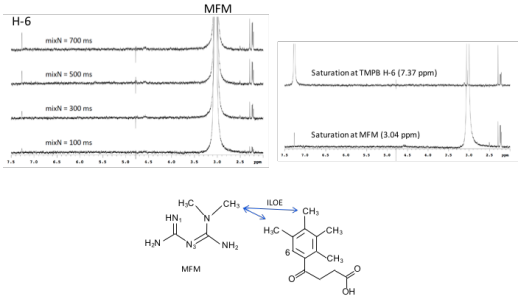

D) 0.1 mM ecDHFR, 5 mM MFM, 5 mM 3-(4-isopropylbenzoyl)propionate

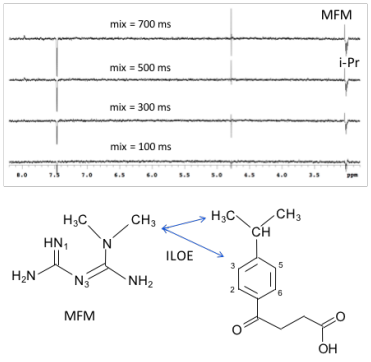

E) 0.1 mM ecDHFR, 5 mM MFM, 30 mM 3,4-dimethoxyhippurate

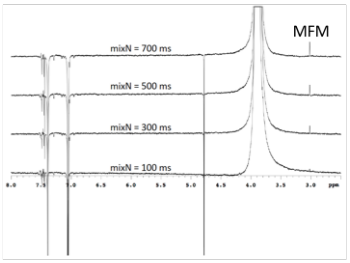

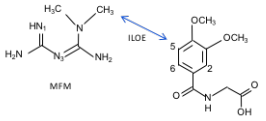

F) 0.1 mM ecDHFR, 5 mM MFM, 5 mM 3-(2,4,5-trimethoxybenzoyl)-propionate

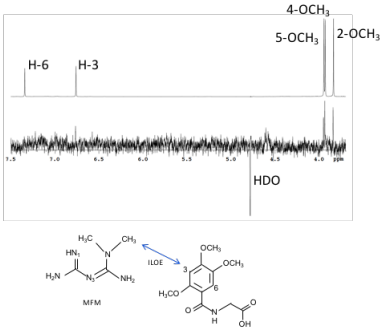

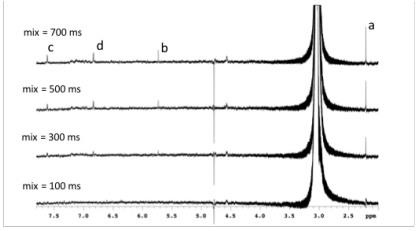

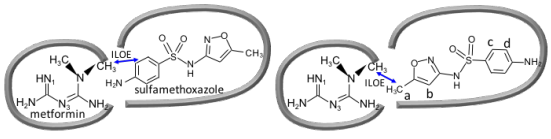

Figure S5. Additional examples of MFM-ILOE interactions with pABG subsite ligands. A) Although no ILOE cross peaks were observed with hippurate under the standard screening conditions, ILOE resonances connecting the MFM resonance with both the aromatic and methyl resonances of 4-methylhippurate were readily observed. B) The ^{1}H NMR spectrum of 4-bromohippurate is surprising, since the ortho and meta resonances overlap (upperspectrum). However, ILOE peaks with hippurate were still observed (lower spectrum). C) The tetramethyl analog shown in the figure is the strongest binding hippurate analog studied, giving both transferred NOE as well as ILOE peaks with MFM. D) For the 4-isopropyl analog the isopropyl methine proton overlaps the MFM methyl resonance. NOE peaks as well as ILOE peaks (of opposite sign) could be observed if the isopropyl methyl resonances were inverted. The MFM methyl resonance appears as a positive shoulder on the inverted I-Pr methine resonance. In this experiment, a more selective inversion required a gaussian cascade rather than a gaussian pulse. E) Trimethoxyhippurate failed to exhibit ILOE resonances, however weak ILOE resonances were obtained with 3,4-dimethoxyhippurate at high concentrations. In this study, the dimethoxy resonances were inverted and a weak ILOE effect on the MFM methyl groups, as well as (negative) intramolecular NOE contributions for the other resonances of the analog, are observed. F) The 2,4,5-trimethoxybenzoyl analog exhibited a very weak aromatic ILOE signal, which required a longer accumulation period for observation. Nevertheless, some ILOE interactions can be observed, particularly for the methoxy protons. The larger ILOE for H-3 compared with H-6 confirms the orientation of this analog in the pABG binding site, and also provides further support for the conclusion that substitutens at the 3- or 5- position (depending on orientation) generally interfere with MFM binding. Assignments of the methoxy resonances is tentative, based on comparison with other analogs studied. G) ILOE connectivity of MFM with sulfamethoxazole. Irradiation of MFM protons at 3.04 ppm produced ILOE responses in both rings. We interpret these results as indicating that the sulfamethoxazole can bind to the pABG site in either of two orientations. Binding probably involves hydrophobic interactions as well as H-bonding to the sulfonamide oxygens.

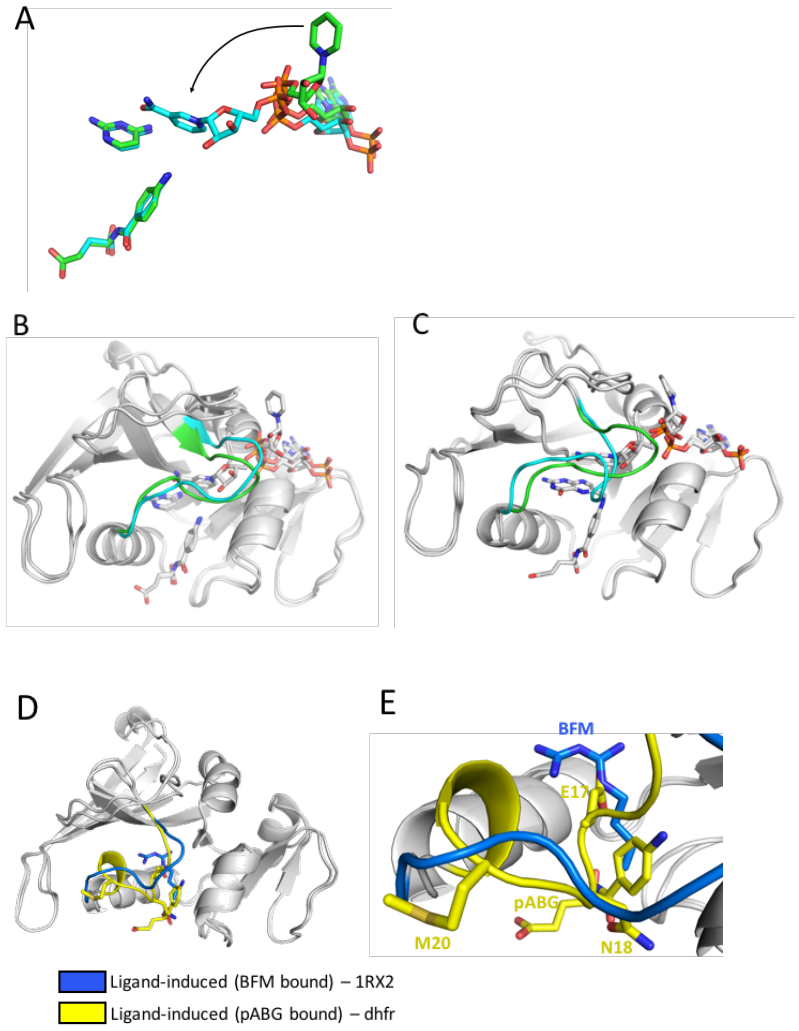

Figure S6. Structural data for ecDHFR-DAP-pABG-NADP$^+$ complex and ecDHFR-pABG complex, showing alternate nicotinamide positions. A) Overlaid ligand positions with the nicotinamide out of the active site (molecule A, green) or in the active site (molecule D, cyan). Overlay optimized the alignment of helix A and consequently the DAP and pABG alignment. B) Overlay shown in panel A, but with the entire ecDHFR enzyme included, and with the Met20 lops color coded in green or cyan. C) Overlaid ribbon diagrams for ecDFHR showing ternary complexes in the closed (green, 1RX2) or occluded (cyan, 1RC4) state. 1RX2 contains bound folate and NADP$^+$; 1RC4 contains bound 5,10-dideazatetrahydrofolate (not shown for simplicity) and NADP$^+$. A comparison of panels B and C indicates that in the DAP-containing structures, the alternate positions of the ribonicotinamide are accommodated with relatively limited, although not identical, closed conformations of the Met20 loop. D) Overlaid ribbon diagrams corresponding to a complex of ecDHFR with BFM and NADP$^+$, and for a low resolution complex with pABG. The Met20 loop is colored in blue and yellow for the two structures. These results suggest that in the presence of pABG, the Met20 loop can adopt a pABG-induced conformation that partially occludes the pteridine binding subsite. This figure illustrates that the loop can interfere with binding of the biguanide; E) expanded view of the overlay in A showing that the Glu17 sidechain may interfere with biguanide binding. Note, however, that in the low-resolution structure, the Glu17 sidechain position was undetermined.

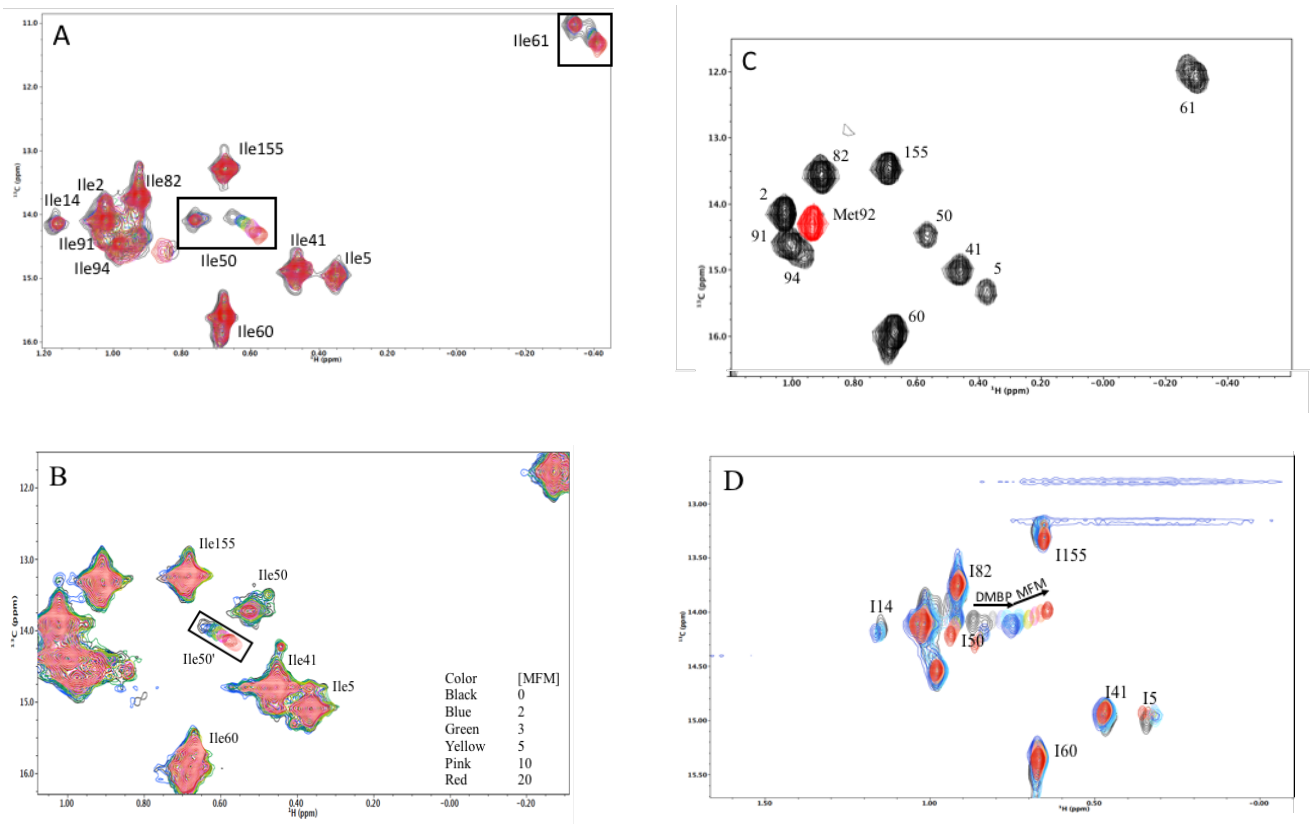

Figure S7. Response of [$^{13}CH_3$-Ile]ecDHFR complexes to metformin. A) Addition of MFM to a sample containing [$^{13}CH_3$-Ile]ecDHFR + 50 mM pABG indicated that the minor Ile50 and Ile61 resonances shift, while the major peaks were invariant. The color-coded MFM concentrations were: 0, black; 2, blue; 3 green; 5, yellow; 10, pink; 20, red. Fitting the shifts of the MFM-sensitive Ile50 and Ile61 resonances gave Kd values of 6.89±0.,56 and 5.36±1.15 mM B) Two Ile50 resonances are still resolved after addition of 2 mM $NADP^+$, and as in panel A, only one is sensitive to MFM addition. A fit of the shift of the MFM-sensitive Ile50 resonance gave K_d = 5.27±0.71 mM. C) The assigned methyl-methyl NOESY spectrum obtained for a sample containing 750 µM U-[^{13}C,^{15}N]ecDHFR + 75 mM pABG + 5 mM $NADP^+$ + 100 mM MFM. In this spectrum, the MFM-sensitive Ile50' resonance position agrees well with the final titration position in the experiment shown in panel B, indicating that at high ligand concentrations, one conformation predominates. Assignment of the resonance labeled Ile50 to an alternate conformation could not be supported by the assignment studies and hence is tentative. D) ^1H-^{13}C HMQC of [$^{13}CH_3$-Ile]ecDHFR serially titrated with DMBP, and then MFM. The color-coded concentrations in mM are: DMBP: 0, black; 5, gray; 10, purple; 20, aqua; 40, medium blue; 75, dark blue. MFM: 0, dark blue; 5, yellow; 10, pink; 20, beige; 40**,** light red; 75, dark red. The titration data for MFM is shown in Figure 2C.

Table S1. Crystallographic data statistics

data set	phenformin	pABG, DAP	pABG, DAP	buformin
unit cell	a=38.61, b=58.87, c=40.15 α=γ= 90°, β =107.54°	a=62.78, b=103.95, c=145.40 α=β=γ= 90°	a=38.60, b=46.12, c=47.98 α=78.04, β= 75.80, γ=75.53	a=73.40, b=58.72, c=38.60 α=γ= 90°, β =107.54°
Pdb Code	5UIH	5UIO	5UIP	5UII
# of crystals	1	1	1	1
Space Group	$P2_1$	$P2_12_12_1$	P1	C2
Resolution (Å)	50.0-1.65	50 – 1.93	50 – 1.90	50 – 1.35
# of observations	122,069	570,644	80,044	175,671
unique reflections	20,763	72,439	23,632	33,675
Rsym(%)(last shell)[1]	8.1 (51.4)	5.8 (47.5)	5.0 (12.7)	10.6 (24.3)
I/σI (last shell)	14.6 (2.1)	18.6 (2.7)	15.1 (7.8)	41.8 (4.0)
Mosaicity range	1.2 - 1.7	0.5 – 0.8	0.8 - 1.4	0.6 – 0.9
completeness(%) (last shell)	99.7 (97.8)	100.0 (99.9)	97.5 (81.2)	98.5 (83.8)
Refinement statistics				
Rcryst(%)[2]	17.8	19.2	15.8	15.9
Rfree(%)[3]	21.6	23.2	19.1	17.4
# of waters	224	621	396	204
Overall Mean B (Å) Protein ligands solvent	 22.5 25.2 32.5	 30.7 31.9 37.7	 22.4 22.4 30.7	 22.9 20.8
r.m.s. deviation from ideal values				31.6
bond length (Å)	0.008	0.005	0.003	0.004
bond angle (°)	1.08	0.85	0.65	0.81
dihedral angle (°)	10.67	15.10	11.44	11.68
Ramachandran Statistics[5]				
residues:				
favored (98%)	98.7	99.1	99.1	99.4
allowed (>99.8%)	1.26	0.9	0.9	0.6

1) Rsym = $\sum (|I_i - \langle I \rangle|) / \sum(I_i)$ where I_i is the intensity of the ith observation and $\langle I \rangle$ is the mean intensity of the reflection.
2) Rcryst = $\sum||Fo| - |Fc|| / \sum|Fo|$ calculated from working data set.
3) Rfree was calculated from 5% of data randomly chosen not to be included in refinement.
4) Ramachandran results were determined by MolProbity[5].

REFERENCES

1. Sawaya, M. R.; Kraut, J. Loop and subdomain movements in the mechanism of Escherichia coli dihydrofolate reductase: Crystallographic evidence. *Biochemistry* **1997,** 36, 586-603.
2. Birdsall, B.; Burgen, A. S. V.; Miranda, J. R. D.; Roberts, G. C. K. Cooperativity in Ligand-Binding to Dihydrofolate-Reductase. *Biochemistry* **1978,** 17, 2102-2110.
3. Venkitakrishnan, R. P.; Zaborowski, E.; McElheny, D.; Benkovic, S. J.; Dyson, H. J.; Wright, P. E. Conformational changes in the active site loops of dihydrofolate reductase during the catalytic cycle. *Biochemistry* **2004,** 43, 16046-16055.
4. Smiley, R. D.; Saxton, A. M.; Jackson, M. J.; Hicks, S. N.; Stinnett, L. G.; Howell, E. E. Nonlinear fitting of bisubstrate enzyme kinetic models using SAS computer software: application to R67 dihydrofolate reductase. *Anal Biochem* **2004,** 334, 204-6.
5. Chen, V. B.; Arendall, W. B.; Headd, J. J.; Keedy, D. A.; Immormino, R. M.; Kapral, G. J.; Murray, L. W.; Richardson, J. S.; Richardson, D. C. MolProbity: all-atom structure validation for macromolecular crystallography. *Acta Crystallogr D* **2010,** 66, 12-21.